Disk Yb:KGW amplifier of profiled pulses of laser driver for electron photoinjector

E. I. Gacheva,[1,*] V. V. Zelenogorskii,[1] A. V. Andrianov,[1] M. Krasilnikov,[2] M. A. Martyanov,[3] S. Yu. Mironov,[1] A. K. Potemkin,[1] E. M. Syresin,[4] F. Stephan,[2] and E. A. Khazanov[1]

[1]*Institute of Applied Physics of the Russian Academy of Sciences, 603950, Ul'yanov Street 46, Nizhny Novgorod, Russia*
[2]*Deutsches Elektronen-Synchrotron, location Zeuthen, D-15738, Platanenallee 6, Zeuthen, Germany*
[3]*European Organization for Nuclear Research, CH-1211, Geneva 23, Switzerland*
[4]*Joint Institute for Nuclear Research, 141980, Joliot-Curie 6, Dubna, Moscow region, Russia*
[*]*gacheva@appl.sci-nnov.ru*

Abstract: We investigated a diode-pumped multipass disk Yb:KGW amplifier intended for amplifying a train of 3D ellipsoidal pulses of a laser driver for a photocathode of a linear electron accelerator. The multipass amplification geometry permitted increasing the energy of broadband (about 10 nm) pulses with a repetition rate of 1 MHz from 0.12 μJ to 39 μJ, despite large losses (two orders of magnitude) introduced by a beam shaper of 3D ellipsoidal beam. The distortions of the pulse train envelope were minimal due to optimal delay between the moment of pump switching on and arrival of the first pulse of the train.

OCIS codes: (140.3280) Laser amplifiers; (140.3615) Lasers, ytterbium; (110.6880) Three-dimensional image acquisition.

References and links

1. Working Group on a European XFEL Facility in Hamburg, *Interim Report of the Scientific and Technical Issues (XFEL-STI)*, Technical Report (DESY, 2005).
2. M. Krasilnikov, F. Stephan, G. Asova, H.-J. Grabosch, M. Groß, L. Hakobyan, I. Isaev, Y. Ivanisenko, L. Jachmann, M. Khojoyan, G. Klemz, W. Köhler, M. Mahgoub, D. Malyutin, M. Nozdrin, A. Oppelt, M. Otevrel, B. Petrosyan, S. Rimjaem, A. Shapovalov, G. Vashchenko, S. Weidinger, R. Wenndorff, K. Flöttmann, M. Hoffmann, S. Lederer, H. Schlarb, S. Schreiber, I. Templin, I. Will, V. Paramonov, and D. Richter, "Experimentally minimized beam emittance from an L-band photoinjector," Phys. Rev. **15**(10), 100701 (2012).
3. K. Tsuchiya, Y. Higashi, H. Hisamatsu, M. Masuzawa, H. Matsumoto, C. Mitsuda, S. Noguchi, N. Ohuchi, T. Okamura, K. Saito, A. Terashima, N. Toge, and H. Hayano, "Cryomodule development for superconducting RF test facility (STF) at KEK," in *Proc. of the 10th European Particle Accelerator Conference (EPAC)*, 506–507 (2006).
4. M. C. Divall, A. Andersson, B. Bolzon, E. Bravin, E. Chevallay, S. Doebert, A. Drozdy, V. Fedosseev, C. Hessler, T. Lefevre, S. Livesley, R. Losito, O. Mete, M. Petrarca, and A. N. Rabiller, "Fast phase switching within the bunch train of the PHIN photo-injector at CERN using fiber-optic modulators on the drive laser," Nucl. Instrum. Meth. Phys. Res. A **659**(1), 1–8 (2011).
5. I. M. Kapchinskij and V. V. Vladimirskij, "Limitations of proton beam current in a strong focusing linear accelerator associated with the beam space charge," in *Proc. of the 2-nd Conf. on High Energy Accelerators and Instrumentation*, 274–288 (1959).
6. M. B. Danailov, A. Demidovich, R. Ivanov, I. Nikolov, and P. Sigalotti, "Performance of the FERMI FEL photoinjector laser," in *Proceedings of FEL*, 358–361 (2007).
7. H. Tomizawa, H. Dewa, H. Hanaki, and F. Matsui, "Development of a yearlong maintenance-free terawatt Ti: Sapphire laser system with a 3D UV-pulse shaping system for THG," Quantum Electron. **37**(8), 697–705 (2007).
8. I. Will and G. Klemz, "Generation of flat-top picosecond pulses by coherent pulse stacking in a multicrystal birefringent filter," Opt. Express **16**(19), 14922–14937 (2008).
9. S. Cialdi, C. Vicario, M. Petrarca, and P. Musumeci, "Simple scheme for ultraviolet time-pulse shaping," Appl. Opt. **46**(22), 4959–4962 (2007).
10. A. Trisorio, C. Ruchert, and C. P. Hauri, "Direct shaping of picosecond high energy deep ultraviolet pulses," Appl. Phys. B **105**(2), 255–261 (2011).
11. Y. Li, S. Chemerisov, and J. Lewellen, "Laser pulse shaping for generating uniform three-dimensional ellipsoidal electron beams," Phys. Rev. Spec. Top.-Accel. Beams **12**(2), 020702 (2009).

#232856 - $15.00 USD Received 22 Jan 2015; revised 19 Mar 2015; accepted 20 Mar 2015; published 6 Apr 2015

12. P. Musumeci, J. T. Moody, R. J. England, J. B. Rosenzweig, and T. Tran, "Experimental generation and characterization of uniformly filled ellipsoidal electron-beam distributions," Phys. Rev. Lett. **100**(24), 244801 (2008).
13. V. V. Zelenogorskii, A. V. Andrianov, E. I. Gacheva, G. V. Gelikonov, M. Krasilnikov, M. A. Mart'yanov, S. Yu. Mironov, A. K. Potemkin, E. M. Syresin, F. Stephan, and E. A. Khazanov, "Scanning cross-correlator for monitoring uniform 3D ellipsoidal laser beams," Quantum Electron. **44**(1), 76–82 (2014).
14. L. M. Frantz and J. S. Nodvik, "Theory of pulse propagation in a laser amplifier," J. Appl. Phys. **34**(8), 2346–2349 (1963).
15. V. I. Talanov, "Propagation of a short electromagnetic pulse in an active medium," Soviet Radiophys. **7**(3), 491–496 (1964).
16. W. Koechner, *Solid-State Laser Engineering (Sixth Revised and Updated Edition)* (Springer, 2006).
17. P. Klopp, *New Yb^{3+}-doped laser materials and their application in continuous-wave and mode-locked lasers (dissertation)* (Humboldt University, 2006).
18. J. Koerner, J. Hein, M. Kahle, H. Liebetrau, R. Seifert, M. Lenzki, S. Pastrik, M. Kaluza, D. Klopfel, S. Keppler, M. Hornung, A. Kessler, and C. Paiva Joao, "Experimental verification of short pulse amplification to the Joule level in Yb:CaF_2," presentation, IOQ Jena, 2010.
19. S. Biswal, S. P. O'Connor, and S. R. Bowman, "Thermo-optical parameters measured in ytterbium-doped potassium gadolinium tungstate," Appl. Opt. **44**(15), 3093–3097 (2005).
20. Eksma Optics, "Yb:KGW and Yb:KYW crystals laser lines and harmonics," http://eksmaoptics.com/out/media/YbKGW.pdf.

1. Introduction

Free electron lasers (FELs) demand for their operation electron beams with high peak current (on the order of kiloampere after several stages of electron bunch compression), a small value of normalized transverse emittance (less than 1 mm·mrad), and small energy spread (~0.1%). Works on generating electron beams with such characteristics are carried out in many research centers worldwide. Examples are FLASH (Germany), SLAC (US), European XFEL, and others.

The most promising sources of electrons in such facilities are injectors with a high-frequency gun and a laser-driven photocathode. With the use of such photoinjectors the possibility to produce beams with parameters needed for FELs was demonstrated. Electron beams in such facilities are modulated in time so that short electron bunches with a duration about units or tens of picoseconds, following with a repetition rate of several megahertz, form relatively long (0.6-10 ms) rectangular trains repeating, in turn, with a frequency of 1-50 Hz [1–4].

The decisive factor in generating beams with small emittance is profiling of the temporal shape of laser driver radiation. For instance, electron bunches with a charge of 1 nC and normalized transverse emittance of 1.4 mm·mrad at the electron energy of 150 MeV were produced on the FLASH FEL photoinjector based on a linear accelerator for Gaussian laser pulses with a RMS duration of 6 ps. An emittance of about 0.7 mm·mrad was obtained at the PITZ photoinjector at DESY in Zeuthen for ~21 ps FWHM pulses trapezoidal in time with ~2 ps front and tail [2]. A further reduction of electron bunch emittance is possible with the use of 3D profiling. Thus, the authors of [5] showed that minimal increase of transverse emittance occurs at acceleration of electron bunches shaped as a 3D ellipsoid (two transverse coordinates and time) with constant electron density inside. Such electron density distribution is called Kapchinskij-Vladimirskij distribution.

The first step in this direction is generating of 3D ellipsoidal laser pulses. The requirements for spatial and temporal structure of the electron beam extend to the corresponding requirements for the structure of the laser radiation arriving at the photocathode. Hereinafter short picosecond pulses will be referred to as micropulses and trains of such pulses will be referred to as macropulses. The micropulse energy needed for injection of bunches with a charge of about 1 nC depends on the photocathode efficiency. For more stable and efficient Cs_2Te photocathodes, the micropulse energy ~1-10 μJ at the wavelength of 0.2-0.3 μm is needed.

Currently, work is underway on putting the laser driver into operation in the linear electron accelerator PITZ. The driver will generate 3D ellipsoidal micropulses at the wavelength of 255-260 nm with the energy of 10-15 μJ, RMS duration of 7 ps and repetition rate of 1 MHz. Identical micropulses will be grouped into macropulses with a duration of 300

#232856 - $15.00 USD Received 22 Jan 2015; revised 19 Mar 2015; accepted 20 Mar 2015; published 6 Apr 2015

μs and a repetition rate up to 10 Hz. The general scheme of the laser driver will be described in section 2 of the paper. Sections 3 and 4 will be concerned, respectively, with theoretical and experimental study of the Yb:KGW amplifier.

2. General scheme of the laser driver

A block diagram of a driver comprising two principal parts: fiber and volume, is presented in Fig. 1. The fiber part includes a fiber Master Oscillator (MO), a fiber stretcher, two multicascade fiber amplifiers (separately for the working and diagnostic channels) and a fiber scanner (a delay line of the diagnostic channel with a rapidly changing length). The MO generates Fourier-limited 200 fs micropulses with a spectrum about 10 nm wide and a repetition rate of 45 MHz. After the fiber stretcher, micropulses are stretched up to 100 ps, retaining their spectral characteristics. This enables their further amplification in the fiber amplifiers without visible influence of cubic nonlinearity on the radiation parameters. At the output of the fiber part, the micropulse energy in each channel is 0.5 μJ at the repetition rate of 1 MHz. The central radiation wavelength is 1030 nm. Also, the fiber part contains three fiber acousto-optical modulators rarefying the continuous micropulse sequence and forming macropulses with controlled repetition rate up to 10 Hz (not shown in Fig. 1). The macropulse envelope is rectangular, i.e., the micropulses inside the macropulse are identical. The micropulse duration in each channel may be varied within 0.2-100 ps range by means of diffraction grating compressors. The compressor in the diagnostic channel compresses micropulses down to 200 fs, and in the working channel down to 20-30 ps.

Further, the radiation from the diagnostic channel arrives at a cross-correlator, and the radiation from the working channel at the disk Yb:KGW amplifier and shaper that forms 3D ellipsoidal pulses. In spite of recently intensively developing pulse shaping techniques the problem of 3D ellipsoidal laser pulse generating isn't solved yet. Some schemes act independently in spatial and time domain and thus allow just 3D cylindrical pulse shaping [6, 7], or focus on time domain only [8–10]. Also there are some attempts to create exactly 3D ellipsoidal laser pulse [11] or directly electron bunch [12], but no result of nC energy level calculating to the electron bunch is achieved. Our approach to laser pulse shaping is truly 3D and has no fundamental limitation in energy scaling. The principal part of the shaper is a zero-dispersion compressor with two diffraction gratings and two spatial light modulators (SLM). SLMs produce masks (amplitude and phase ones) in the spatial and spectral regions, thus permitting control of the space-time characteristics of the chirped radiation. After the second pass of the amplifier located in the scheme next to the shaper, the micropulse energy attains the value of 50 μJ which, with allowance for the efficiency of conversion into harmonics, must be sufficient for the required 1-10 μJ at the fourth harmonic.

After the second pass of the disk amplifier, the radiation is transmitted to the second-harmonic generator and then to the fourth-harmonic generator. For efficient conversion of broadband radiation into harmonics, the scheme of angular chirping is used. The radiation acquires angular chirp during passage of the dispersion prism located before the nonlinear crystals. The harmonic generation will be described in more detail in a separate paper. For monitoring the space-time 3D shape of the micropulse, part of the radiation is transmitted from the laser driver output to a cross-correlator. The cross-correlator is described in detail in [13].

#232856 - $15.00 USD Received 22 Jan 2015; revised 19 Mar 2015; accepted 20 Mar 2015; published 6 Apr 2015

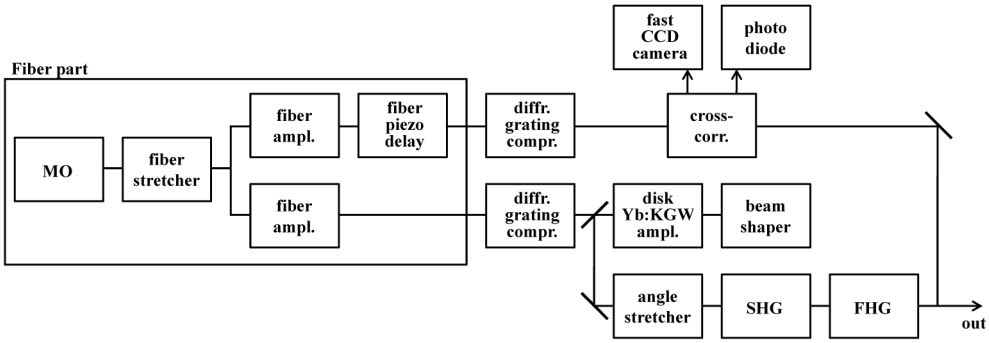

Fig. 1. Laser driver block diagram.

On propagation in free space and in transparent dielectrics, the shape of the 3D ellipsoidal pulse is distorted. Generally speaking, it is impossible to produce an ideal 3D ellipsoidal micropulse with constant intensity within the ellipsoid surface and zero intensity outside as, due to infinitely sharp edges, it must have an infinitely broad spectrum both in time and in space. Therefore, we assume that its edges are blurred and the spectrum width is finite. For 1 ps width of ellipsoid's temporal fronts, simple estimations of such pulse smearing in a dispersive medium show that it may propagate tens of meters in optical glass or hundreds of kilometers in air without visible distortions. Thus, there is no need to compensate the dispersion. To prevent ellipsoid distortions due to diffraction, we use image retranslation through the entire optical path by means of Kepler telescopes. Smearing of the ellipsoid borders in transverse spatial coordinates slightly reduces requirements for accuracy of image transmission.

In the present research, we use KGW crystals activated by Yb^{3+} ions as an active medium of a disk amplifier. The active medium is pumped by a diode laser with multimode fiber output operating in the 935-940 nm wavelength region. This active medium allows amplifying signals with spectrum width of ~10 nm at central wavelength of 1030 nm without visible distortions. Due to some peculiarities of the Yb^{3+} ion energy levels arrangement the physical model of the amplifier deserve special consideration.

3. Theoretical model of the amplifier

3.1 The idea of prepumping

As was mentioned above, in the described laser system macropulses with a duration of 300 μs must be amplified, with the envelope retaining its rectangular shape in time. The macropulse duration is close to the lifetime of the upper laser level of ytterbium in KGW crystal (τ = 320 μs). Consequently, we can use in calculations of the amplifier neither the exact Franz-Nodvik-Talanov solution for short laser pulses [14, 15], nor the exact solution for the stationary case when the output I_{out} and input I_{in} intensities are related by the transcendental equation

$$\frac{I_{out} - I_{in}}{I_s} = ln\left(G_0 \frac{I_{in}}{I_{out}} \right), \tag{1}$$

where I_s is the intensity of transition saturation, $G_0 = exp(\alpha_0 L)$ is the small signal gain for steady-state amplification, and L is the amplifier length. In this case, we will make use of the equation for a linear gain α [16]

$$\tau \frac{d\alpha}{dt} = \frac{ln(G_0)}{L} - \alpha - \frac{I_{in}}{LI_s}\left(e^{\alpha L} - 1\right), \tag{2}$$

Equation (1) being its stationary solution.

#232856 - $15.00 USD Received 22 Jan 2015; revised 19 Mar 2015; accepted 20 Mar 2015; published 6 Apr 2015

Apparently, if the pump pulse (we assume it to be rectangular) starts simultaneously with the macropulse, then the gain will first grow in time. Hence, for obtaining a rectangular output macropulse, the input macropulse should be profiled. This step may be avoided by using prepumping when the pump pulse starts before the input macropulse. However, if the amplified macropulse arrives too late, when the gain is larger than its stationary value and starts to decrease, then macropulse profiling will be demanded again. For the rectangular laser macropulse not to be distorted during amplification, it is important to correctly choose the delay time t_0 between the beginning of the pump pulse and of the amplified macropulse, i.e., the moment of arrival of the first micropulse at the amplifier.

Up to time t_0, the input intensity $I_{in} = 0$, and from Eq. (2) we obtain

$$\alpha L = ln\left(G_0\right)\left(1-\exp\left(-t/\tau\right)\right). \tag{3}$$

From physical considerations it is clear that the input macropulse must arrive at time t_0, when the gain α reaches the value at which $d\alpha/dt$ in Eq. (2) is equal to zero. In this case, the balance between the increase of inversion by the pump and the decrease of inversion by the input signal and spontaneous emission is established. Thus, the value of I_{out} will not change in time and the amplified macropulse will not be distorted. If the input macropulse arrives before t_0, the output macropulse will grow until it reaches its stationary value. If the input macropulse arrives later than t_0, when the gain will be larger than the stationary value, the output macropulse will decrease down to its stationary value. By zeroing the derivative in Eq. (2) and substituting into it Eq. (3), we obtain an equation for t_0 with solution in the form

$$t_0 = -\tau \ln\left(\eta\right), \tag{4}$$

where $\eta = (I_{out}-I_{in})/I_s/ln(G_0)$ is the amplifier efficiency, i.e., the ratio of the power withdrawn by the pulse from the amplifier to the maximum possible withdrawn power (when I_{in} tends to the infinity). Here, the output I_{out} and the input I_{in} intensities are average in time on macropulse duration, i.e., $I_{in,\,out} = w_{in,\,out}/\Delta t$, where w is the micropulse energy density and Δt is the time between two micropulses.

The expression Eq. (4) may also be obtained by equating the decrease of the energy stored in the medium due to micropulse amplification (w_{out}-w_{in}) to the increase of the energy stored during the time between two micropulses $\Delta t L w_s d\alpha/dt$, where $w_s = I_s\tau$ is the saturation energy density. With the use of this approach it is clear that Eq. (4) holds true for an arbitrary number of passes through the amplifier and for an arbitrary number of successive amplifiers, if α_0 is understood as a stationary small signal gain per one pass through all the amplifiers.

3.2 Balance equations for a quasi-four-level medium

An active Yb^{3+} ion is an example of a quasi-four-level medium. The electron distribution within the upper and lower multiplets is described by the Boltzmann formula. Widths of these multiplets are so small that at room temperature the populations of the upper pump and lower laser levels cannot be neglected. Pump reemission and amplified signal reabsorption are observed. The balance equations relating the population of laser medium energy levels and photon density in the medium have the form [17]:

$$\frac{dI_p}{dz} = NI_p\left(\beta\sigma_{em}\left(\lambda_p\right)-\left(1-\beta\right)\sigma_{ab}\left(\lambda_p\right)\right) \tag{5}$$

$$\frac{dI_l}{dz} = NI_l\left(\beta\sigma_{em}\left(\lambda_l\right)-\left(1-\beta\right)\sigma_{ab}\left(\lambda_l\right)\right) \tag{6}$$

#232856 - $15.00 USD Received 22 Jan 2015; revised 19 Mar 2015; accepted 20 Mar 2015; published 6 Apr 2015

$$\frac{d\beta}{dt} = (1-\beta)\left(\sigma_{ab}(\lambda_p)\frac{I_p}{\hbar\omega_p} + \sigma_{ab}(\lambda_l)\frac{I_l}{\hbar\omega_l}\right) - \\ -\beta\left(\sigma_{em}(\lambda_p)\frac{I_p}{\hbar\omega_p} + \sigma_{em}(\lambda_l)\frac{I_l}{\hbar\omega_l}\right) - \frac{\beta}{\tau} \quad (7)$$

If we denote by N_1 and N_2 the sum populations in the upper and lower multiplets respectively, the concentrations of active ions in the medium is $N = N_1 + N_2$. Thermolization within the multiplets in this model is regarded to be instantaneous [17]. The inversion parameter is introduced as $\beta = N_2/N$. I_p and I_l are the pump and the signal intensities. The system of balance equations (Eqs. (5)-(7)) takes into account the processes of pump absorption (with cross-section $\sigma_{ab}(\lambda_p)$), pump reemission ($\sigma_{em}(\lambda_p)$), signal emission at the laser wavelength ($\sigma_{em}(\lambda_l)$), signal reabsorption ($\sigma_{ab}(\lambda_l)$), and spontaneous decrease of inversion (with characteristic time τ = 320 μs). Our theory is based on a radially symmetric beam model, the input data are approximations of the transverse distributions of real pump and laser beams. Before passing over to results of numerical simulation and comparison of the theory and the experiment, let us consider in more detail the specific features of experimental implementation of the amplifier.

4. Experimental study of the Yb:KGW amplifier

4.1 Optical scheme of the amplifier

Figure 2 shows the optical scheme of the disk amplifier used in our experiments. The active elements (AEs) made of Yb:KGW crystals, 7x7x3 mm in size were cut in the $m \parallel \vec{E}_{pump} \parallel \vec{E}_{signal}$, $g \parallel z$ orientation. The direction of pump and signal polarization was chosen so as to ensure maximum signal amplification and maximum absorption of the pump. The 3% Yb^{3+} concentration in AEs allowed absorbing 80-90% of pump power in one V-pass in an unsaturated regime. The front surface of AE had an antireflecting coating for the signal and pump wavelengths. The back surface had a 100% dielectric mirror, also for the signal and pump. Hereinafter, the V-pass will be regarded to be the radiation passage through the laser medium forward and backward on reflection from the back surface. In *n* full passes of the amplifier the radiation makes *(n + 1)* V-passes around AE1 and *n* V-passes around AE2.

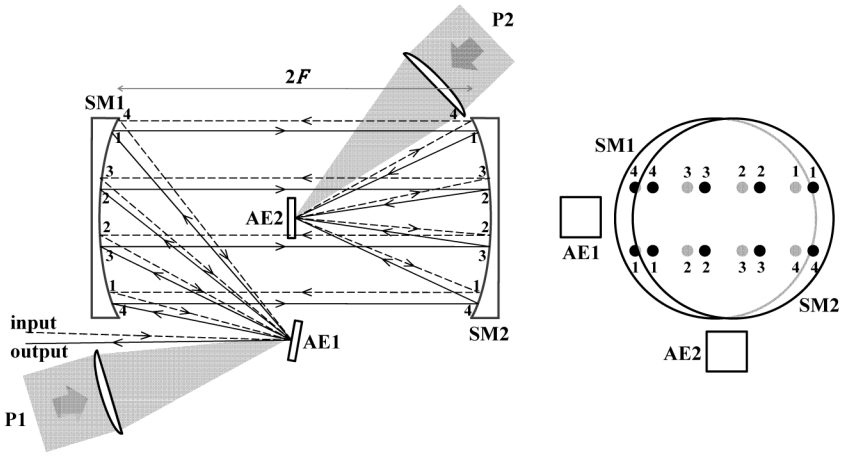

Fig. 2. Optical scheme of the Yb:KGW amplifier (top view – left; side view – right): AE1, AE2 – active elements made of Yb:KGW crystal; SM1, SM2 – spherical mirrors with focus *F*; P1, P2 – two pump channels; the numerals denote the numbers of passes in the amplifier; the solid line is for the upper row of rays, the dashed line is for the lower row of rays.

#232856 - $15.00 USD Received 22 Jan 2015; revised 19 Mar 2015; accepted 20 Mar 2015; published 6 Apr 2015

The average power input to the AEs is relatively small (about 10 W in the pump and 0.2 W only in the signal). Therefore, a laser head with room-temperature water cooling (Fig. 3) was constructed to cool the AEs. Thermal contact between AE and laser head was established through heat conducting paste. Circulation of distilled water in the laser head was provided by the chiller system LAUDA WK500. Water temperature was maintained to an accuracy of ± 0.5 degrees.

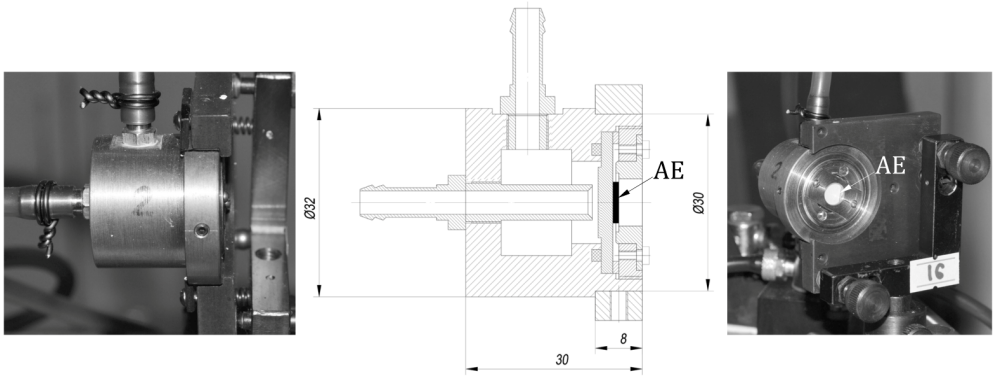

Fig. 3. Laser head with water cooling.

The AEs were pumped by a diode laser operating at the wavelength of 938.5 nm (Laserline, LDM 2000-100) with 2 kW maximum power and a multimode fiber output. As polarized pumping is required for Yb:KGW crystals, we used the following scheme. The depolarized radiation from the end of a 1 mm thick light guide was collimated by a 10 cm lens and on passing the dielectric polarizer was divided into two beams of equal power with orthogonal polarizations. After that, the beams were forwarded to their AEs (AE1 and AE2 in Fig. 2). The pump polarization of AE2 was turned by 90 degrees by means of a half-wave plate. The beam diameter after collimation was 42 mm. Despite the great number of transverse modes, the pump beam of such a large diameter was readily transmitted over distances of 3-4 meters, spreading up to 50 mm. The lens with a focal length of 20 cm, focusing the pump in the AEs, formed a twice magnified image of the end of the fiber (Fig. 4).

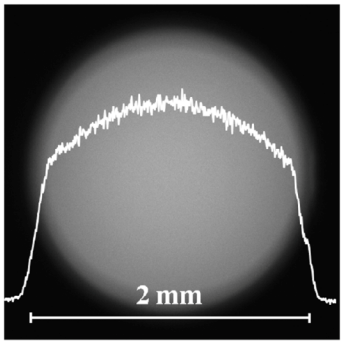

Fig. 4. Transverse distribution of pump intensity in the AE plane.

The optical scheme of the amplifier (Fig. 2) is designed so that the image from AE1 is transferred to AE2 by means of spherical mirrors SM1 and SM2. Thereto, AE1 was placed in the focal plane of SM1 (mirrors with a diameter of 60 mm and a curvature radius of 830 mm were used in our experiments), and AE2 was placed in the focus of SM2. The distance between the mirrors was double focal distance, i.e., the amplifier geometry repeated that of the Kepler mirror telescope. As was mentioned above, accurate imaging is demanded for

#232856 - $15.00 USD Received 22 Jan 2015; revised 19 Mar 2015; accepted 20 Mar 2015; published 6 Apr 2015

preserving the transverse structure of 3D ellipsoidal pulses. One of the spherical mirrors (SM1) and one of the laser heads with AE1 were installed on longitudinal micrometer translators. By comparing input and output transverse distributions and adjusting SM1 and AE1 longitudinal positions to an accuracy of 0.1 mm we could transfer image throughout the scheme (the optical length of the amplifier in the 4-pass scheme was about 32 m).

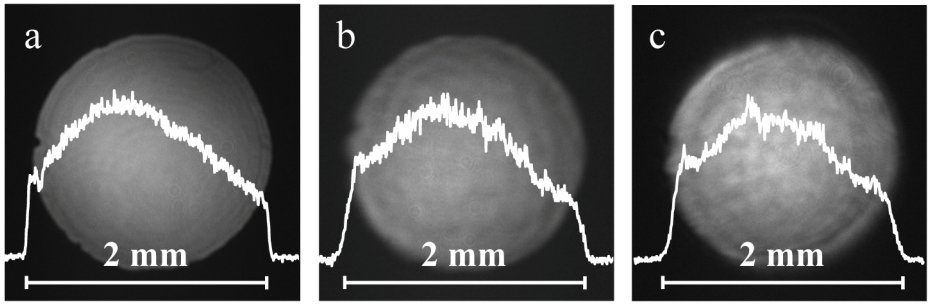

Fig. 5. Transverse distribution of laser radiation in imaging planes: (a) before the amplifier; (b) after a single full pass of the amplifier (9 V-passes); (c) after two full passes of the amplifier (18 V-passes).

To assess diffraction distortions introduced by the amplifier optical scheme we replaced the AEs by mirrors (the quality of Yb:KGW material also affects transverse intensity distribution). Figure 5 presents pictures for initial transverse distribution (a), after a single full pass of the amplifier (b), and after two full passes (c). (Here, the full pass of the amplifier is understood as passage of a 4-pass scheme.) The image from the hard aperture cutting the Gaussian beam coming from the fiber part was transported to the amplifier input. Such a distribution with sharp edges contains many high spatial harmonics and is an illustrative example of the accurate imaging problem. After the first pass, the image acquired a ring inside its edge, indicating that the optical amplifier scheme started to cut the harmonics. After the second pass, small-scale distortions were visible, that had evidently been caused by nonuniform restriction of transmission of laser radiation high spatial harmonics.

As reflections in the Kepler mirror telescope occur at certain angles in meridional plane (the plane on the left of Fig. 2), astigmatism arises in the beam. To correct astigmatism, AE2 should be placed so (Fig. 2, on the right) that reflections in the meridional plane alternate with reflections at the same angles in the sagittal plane [18]. In our scheme, the number of V-passes of AE1 (reflections in the meridional plane) per single full pass of the amplifier is always one more than the number of V-passes of AE2 (reflections in the sagittal plane), hence, the compensation of astigmatism is incomplete. For assessment of the astigmatism arising in the laser beam after the first pass of the amplifier we measured the diameter of the transverse intensity distribution in the x and y directions near the focal plane of the lens with a focal length of 42 cm. One can see in Fig. 6 that the astigmatism in the beam is insignificant. The 3D beam shaper placed between the forward and backward passes through the amplifier (not shown in Fig. 2), besides other manipulations with intensity distribution, turned the beam by 90° around the propagation axis. So, the residual astigmatism measured after the forward pass was compensated on the backward pass.

The maximum number of passes over the AEs in the scheme in Fig. 2 is determined from geometrical considerations. Namely, it depends on the spherical mirror aperture and on the distance which the beam that has passed by the mirror (e.g., an input beam) should be separated by from the beam hitting the edge of this mirror without diffraction distortions. Distances between passes on the spherical mirrors are equal automatically. The maximum number of passes achieved in the present work was 6V-passes over AE1 and 5V-passes over AE2 per one full pass of the amplifier (5-pass scheme).

It should be taken into consideration that such a multipass amplifier scheme may act as a resonator in case of inaccurate adjustment or large enough parasitic scattering. In our

#232856 - $15.00 USD Received 22 Jan 2015; revised 19 Mar 2015; accepted 20 Mar 2015; published 6 Apr 2015

experiments, inaccurate adjustment of the scheme sometimes resulted in self-excitation of the amplifier. The more passes, the more accurate the adjustment must be.

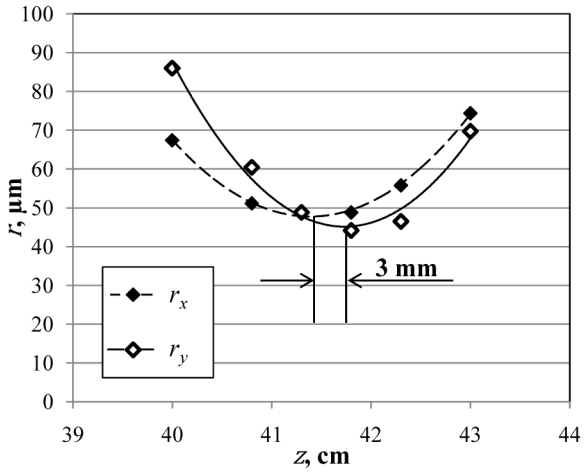

Fig. 6. Beam radius *r* along transverse *x* and *y* coordinates in the beam waist formed by the lens with focal distance 42 cm after the first pass of the amplifier.

4.2 Energy characteristics of the amplifier

The dependence of pump absorption per one V-pass over a 3 mm Yb:KGW crystal on the temperature of pump laser diodes for different polarizations is plotted in Fig. 7. The pump wavelength in that case varied within 934–938.5 nm. The spectrum width persisted to be about 3 nm. The experiment did not reveal any dependence of pump absorption on AE temperature in the 16–26°C range. It is seen in Fig. 7 that in unsaturated regime 85% of pump is absorbed in the AEs. At maximum pump power, this amount decreases to 70% due to saturation (Fig. 8, experiment).

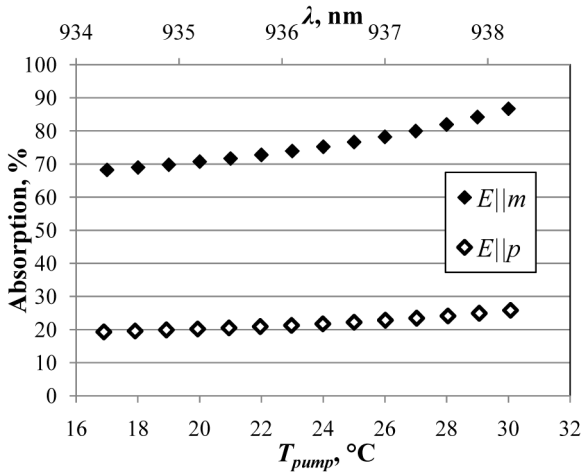

Fig. 7. Pump absorption per single V-pass in AE *versus* laser diode temperature and pump wavelength.

#232856 - $15.00 USD Received 22 Jan 2015; revised 19 Mar 2015; accepted 20 Mar 2015; published 6 Apr 2015

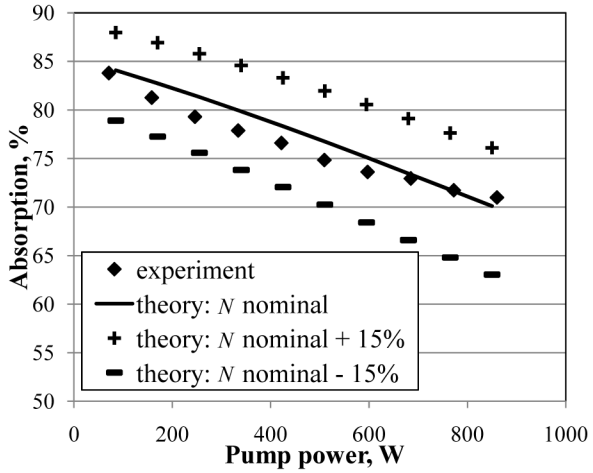

Fig. 8. Absorption of 3% Yb:KGW crystal in m-polarized pump *versus* incident radiation power. Pump spot diameter 2 mm.

In the absence of signal, modeling of pump absorption dynamics in Yb:KGW reduces to joint solution of Eqs. (5) and (7). The difficulty in building a theory for an Yb:KGW crystal is lack of exact data on values of process cross-sections. For solving the problem without an input signal we must know parameters $\sigma_{ab}(\lambda_p)$ and $\sigma_{em}(\lambda_p)$, with the second cross-section being much less than the first one. Let us assume $\sigma_{em}(\lambda_p) = 0$ and, first, find $\sigma_{ab}(\lambda_p)$. The theoretical curve for $\sigma_{ab}(\lambda_p) = 1.7 \cdot 10^{-20}$ cm^2, $N = 1.89 \cdot 10^{20}$ cm^{-3} (corresponding to 3% doping level declared in the passport) is presented in Fig. 8 (theory: N nominal). To understand the agreement between the theoretical and experimental results, let us make a simple evaluation of error. The bench mark of our studies of the transition cross-sections in Yb:KGW was the paper [19], where it was stated that doping level of crystals made in EKSMA is known to an accuracy of ± 15%. We cannot ensure a better accuracy for our crystals. Let us plot two more theoretical curves for $N = 1.89 \cdot 10^{20}$ cm^{-3} ± 15%, other parameters being the same (Fig. 8, theory: N nominal + 15%; theory: N nominal - 15%). The area between these curves is the tolerance region. The experimental curve is inside it, so we can say that the theory agrees with the experiment. The theoretical curve with the initial value of N and $\sigma_{em}(\lambda_p) = \sigma_{ab}(\lambda_p)/10$ (we remind the reader that $\sigma_{em}(\lambda_p) << \sigma_{ab}(\lambda_p)$) is slightly apart from the curve with $\sigma_{em}(\lambda_p) = 0$ and lies inside the tolerance region. Our accuracy is insufficient for determining the small parameter $\sigma_{em}(\lambda_p)$, so in further calculations we will take it as equal to zero.

In the absence of pumping, an Yb:KGW crystal is a strong absorber at the laser wavelength. For example, the measured transmission of a "cold" amplifier per a single full pass of the 4-pass scheme was only 40%. Comparison of results of that measurement with solution of the problem of signal absorption in unpumped medium gave $\sigma_{ab}(\lambda_l) = 0.084 \cdot 10^{-20}$ cm^2.

The measured linear gain ($\alpha = 1/L \cdot ln(W_{out}/W_{in})$, where $L = 0.6 \cdot (2n + 1) \cdot 2$ cm is the total length of the active medium in n-pass scheme, for $n = 5$ $L = 13.2$ cm) in 5-pass scheme as a function of the total pump power is depicted in Fig. 9. At maximum power, the energy gain was 550, and the output micropulse energy was 67 μJ. Simulation of the complete amplification problem Eqs. (5)-(7) enables finding the last cross-section of the process $\sigma_{em}(\lambda_l) = 0.67 \cdot 10^{-20}$ cm^2 as a fitting parameter. The corresponding theoretical curve is in a good agreement with the experiment (Fig. 9). The substitution of the obtained theoretical values into formula Eq. (4) gives the prepump time $t_0 = 580$ μs, which also agrees well with the experimental value of 600 μs (see subsection 4.4). However, it is worth noting that the theory did not take into account inhomogeneities of the transverse beam distribution arising due to a poor quality of Yb:KGW crystals. Therefore, it is very difficult to determine accuracy of the obtained value of $\sigma_{em}(\lambda_l)$.

#232856 - $15.00 USD Received 22 Jan 2015; revised 19 Mar 2015; accepted 20 Mar 2015; published 6 Apr 2015

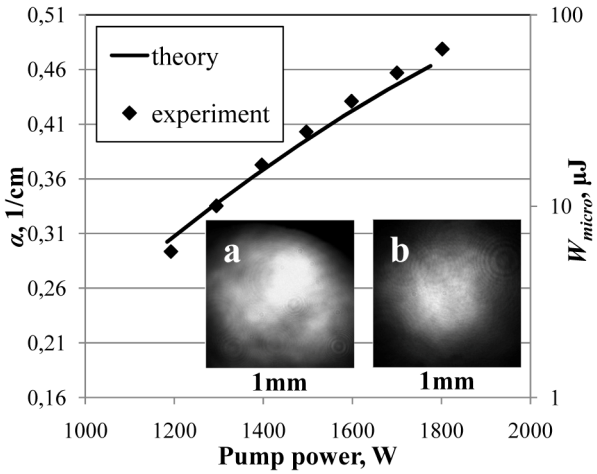

Fig. 9. Linear gain and energy of the output macropulse *versus* pump power at the energy of the input micropulse of 0.12 μJ without 3D beam shaper. In the insets: transverse intensity distribution at the amplifier output at 1800 W pump without 3D beam shaper (output micropulse energy 67 μJ) (a), and with 3D beam shaper (output micropulse energy 39 μJ) (b).

A 3D beam shaper located between the forward and backward passes through the amplifier (not shown in Fig. 2) has the transmission coefficient 12.6% per pass, i.e., only 1.6% per two passes. In the experiment with beam shaper at maximum pump, other conditions being the same, we obtained the gain of 290 and micropulse energy of 39 μJ. The gain including the compensation of losses in the beam shaper is 18000.

4.3 Spectral measurements

The luminescence spectrum of an Yb:KGW crystal in m-polarization has a peculiar three-hump profile (see, e.g., [19, 20]). The spectra obtained for the crystals and pump source used in the present work are shown in Fig. 10. The third maximum at the longest wavelength was chosen for operation. Gain at this maximum is the smallest of the three but sufficient for our problem. At the same time, because of the smallest amplitude and the largest bandwidth of the third maximum, spectrum distortions of the amplified radiation were minimal, which is a critical requirement for amplification of 3D ellipsoidal pulses.

As the shapes of the luminescence and the absorption spectra are not exactly a plateau around 1030 nm (both the maxima are on the blue side of this wavelength), the radiation spectrum was greatly distorted during passage through the cold amplifier and on amplification. The spectra of the laser radiation incident on the amplifier and after passing through the cold and hot amplifier are presented in Fig. 11. It is clear from this figure that the cold amplifier shifted the radiation maximum to the red (by 2-3 nm in our case), and the hot amplifier shifted the radiation maximum to the blue (by about 6-8 nm).

#232856 - $15.00 USD Received 22 Jan 2015; revised 19 Mar 2015; accepted 20 Mar 2015; published 6 Apr 2015

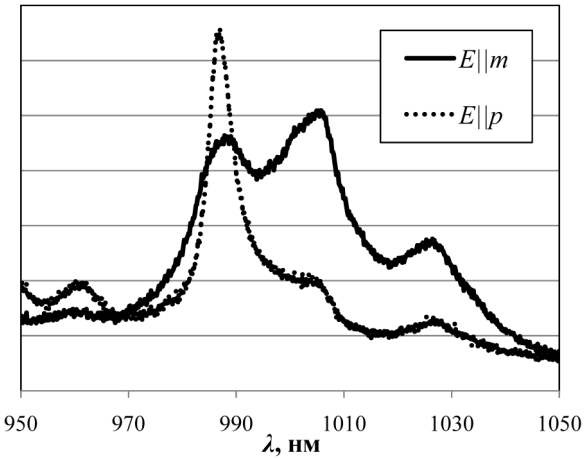

Fig. 10. Luminescence spectra of Yb:KGW crystal in different polarizations. The spectra are not normalized.

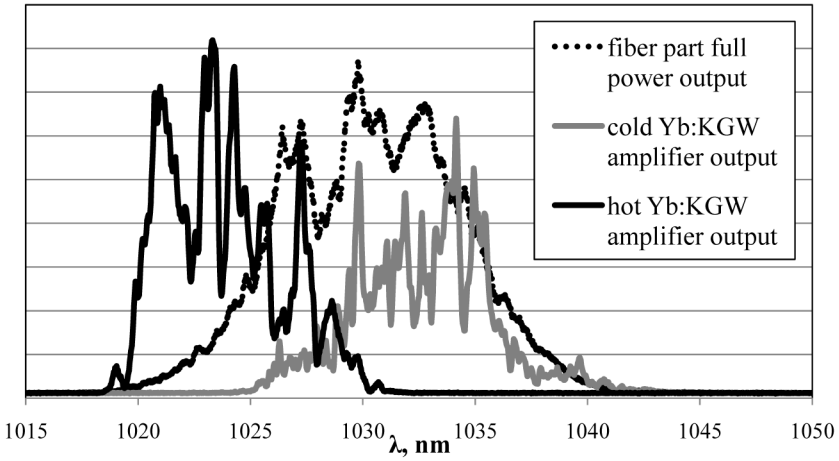

Fig. 11. Spectra of incident laser radiation and of radiation transmitted through the amplifier. The spectra are not normalized.

4.4 Macropulse shape distortions

For amplification of rectangular macropulses, we used the prepumping technique described above. According to this technique, to avoid distortion of macropulse shape, it should be transmitted to the amplifier with a delay Eq. (4) relative to the arrival of the rectangular pump pulse. The macropulse oscillograms corresponding to different delays t are presented in Fig. 12. If the time of macropulse arrival at the amplifier $t<t_0$, where t_0 was found from Eq. (4), the distortion had the increasing profile; if $t>t_0$, then the distortion had the decay profile, and only at $t = t_0$ the macropulse shape was not distorted.

#232856 - $15.00 USD Received 22 Jan 2015; revised 19 Mar 2015; accepted 20 Mar 2015; published 6 Apr 2015

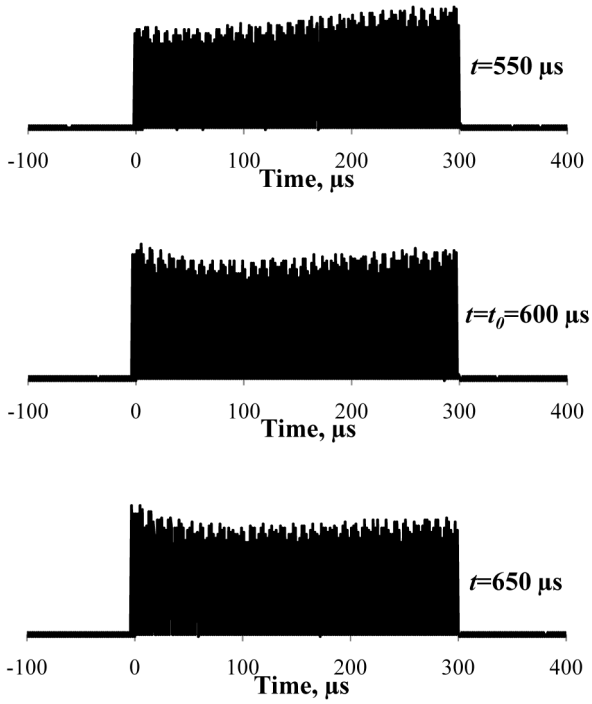

Fig. 12. Oscillograms of amplified macropulses corresponding to different times of prepumping. Small-scale modulation of the oscillograms occur because of digitization discreteness.

5. Conclusion

Within the framework of the research aimed at creating a laser driver for an electron photoinjector with a 3D ellipsoidal pulse, we have constructed a laser amplifier intended for amplification of identical picosecond 3D profiled pulses with a central wavelength of 1030 nm grouped into trains. We have used a multipass scheme comprising a spherical mirror Kepler telescope transmitting the image between two active elements, which the beam with sharp edges runs through without significant diffraction distortions. Due to arranging reflections to different active elements in orthogonal planes, beam astigmatism has been compensated. Amplification at the lowest maximum of the luminescence spectrum enabled obtaining minimal distortion of the spectrum and, hence, of the chirped pulse time profile. To preserve the rectangular shape of the pulse train envelope, prepumping technique has been used.

Acknowledgments

This work was supported in part by the Ministry of Education and Science of the Russian Federation under Contract No.14.Z50.31.0007 and RFBR project Nº13-02-91323 СИГ_а "Application of 3D ellipsoidal cathode laser pulses for high brightness photo injector optimization".

#232856 - $15.00 USD Received 22 Jan 2015; revised 19 Mar 2015; accepted 20 Mar 2015; published 6 Apr 2015